

Mixing Dynamics and Scalar Dissipation Rate in Split-Injection Gaseous Jets

Dong-hyuk Shin¹ and Edward S. Richardson*¹

¹Faculty of Engineering and the Environment
University of Southampton
Highfield Campus Southampton, SO17 1BJ, United Kingdom

Abstract

Split fuel injection is studied by Direct Numerical Simulations (DNS) to characterize the entrainment and scalar dissipation in turbulent gaseous jets. The mixing physics identified in this study are important for the understanding of split-injection compression-ignition engine operation, in which mixing rates and fuel residence time control the rate of heat release and pollutant formation. Three injection scenarios are compared: a starting jet, a stopping jet, and a restarting the fuel jet. It is observed that the entrainment is suppressed or enhanced when the jet accelerates or decelerates respectively, in agreement with previous studies. The results show that the one-dimensional entrainment model by Musculus (Journal of Fluid Mechanics 638 (2009) 117-140) provides a good qualitative description for the entrainment in the stopping jet. It is found that the suppression and enhancement due respectively to a starting and a stopping jet can be superimposed to give an estimate for the entrainment in the restarted jet simulation. Scalar dissipation rate is found to increase or decrease by one order of magnitude as the jet accelerates or decelerates respectively. The wake of the stopping jet reduces the scalar dissipation rate in the following restarting jet, implying that the dissipation rate from the stopping jet and the starting jet are not additive, and highlighting the different dynamics of the large and small scale mixing processes described by entrainment and scalar dissipation respectively.

Introduction

While the fluid dynamics of steady jets have been studied extensively and are well characterized, the mixing processes in transient jets are not well understood. The overall rate of entrainment of ambient fluid into the jet is important in many transient-jet mixing applications. This study is motivated by the application of transient-jets to fuel injection in compression ignition (e.g. Diesel) engines in which scalar dissipation and the fuel residence time are also important factors in the evolution of the combustion process.

Several studies have shown that entrainment is reduced in accelerating jet flow [1], and the converse is observed in decelerating jets [2,3]. These entrainment effects have been attributed to the changing amount of jet fluid and vorticity available to feed the growth of large structures, so that the rate of ambient fluid entrainment adjusts in compensation. Musculus [2] developed a one dimensional model for the evolution of the cross-stream integrated momentum flux \dot{M} in a decelerating jet. Assuming that the velocity profile in the unsteady-jet remains self-similar and neglecting axial interactions he obtained the following wave equation,

$$\frac{\partial \dot{M}}{\partial t} = -2\alpha \frac{\sqrt{\dot{M}}}{x - x_0} \frac{\partial \dot{M}}{\partial x} \quad (1)$$

where, x_0 is the origin of the self-similarity and α is $\cot(\theta/2)\sqrt{\beta/\rho\pi}$, and θ , β and ρ are the jet spreading angle, the radial velocity shape factor, and the density respectively.

The wave equation developed by Musculus predicts that, in the decelerating portion of the jet, the entrainment rate relative to the local concentration of injected fluid is

three times greater than in a steady-state turbulent jet. The model is in qualitative agreement with velocity measurements in a gravity-driven water jet [4] that imply at least a two-fold increase in the dilution rate in the decelerating region of the jet. The model also explains experimental observations that deceleration waves increase the rate of dilution in Diesel fuel jets [5,6].

The practical implication for direct-injection compression-ignition engines is that decreasing the fuel flow rate rapidly generates a wave that dilutes and slows the fuel flow, enhancing soot burn out and reducing the penetration of fuel towards the cylinder walls. On the other hand, if less mixing is desired after the ending transient, such as when the fuel mixture becomes too lean to achieve complete combustion in Diesel engines [5], the deceleration rate may be reduced.

The interaction between successive injection pulses has been investigated using Large Eddy and Reynolds Averaged modelling approaches by Anders et al. [7]. Pending confirmation from experimental or Direct Numerical Simulation data, the model predictions suggest that the mean flow field and turbulence induced by the preceding injection pulse both influence the mixing and penetration of the following pulse. This interaction between successive injection pulses is also expected to contribute to the entrainment dynamics in direct fuel-injected engines that employ split injection.

In addition to the entrainment of oxidizer into the fuel jet, Diesel engine combustion also depends on the local rates of molecular mixing between fuel and oxidizer. The scalar dissipation rate ($\chi_Z = 2D_Z \nabla Z \cdot \nabla Z$) characterizes the local mixing between the jet fluid and the ambient fluid, where Z is the mixture fraction (i.e. a passive scalar with a value of unity in the jet fluid and zero in the ambient fluid) and D_Z is the molecular

* Corresponding author: e.s.richardson@soton.ac.uk
Proceedings of the European Combustion Meeting 2015

diffusivity of mixture fraction. High values of scalar dissipation rate retard the progress of autoignition [8] so that ignition and flame stabilisation usually occur in regions of low scalar dissipation. Recent laboratory measurements illustrate that the scalar dissipation rate is elevated at the leading edge of an impulsively started jet, compared to an equivalent continuous jet [9] but analysis of the scalar dissipation rates during split injection have not been reported based on full-resolution data.

The residence time is important in autoignitive flows since, to leading order, the fluid ignites when the residence time of the most-reactive mixture exceeds the ignition delay time [8]. Split-injection provides a mechanism through which to modify the distribution of residence time in an engine and thereby control the location and timing of ignition events during an engine cycle. Split injection presents a challenge for common mixture fraction-based combustion models [10] since mixture fraction does not distinguish between fuel injected at different times. In flamelet modelling, Hasse and Peters [11] have used two mixture fractions Z_1 , Z_2 to indicate fuel from two discrete injection events, leading to a two-dimensional flamelet model. The cross dissipation rate $\chi_{12} = 2D_Z \nabla Z_1 \cdot \nabla Z_2$ appears in Hasse's model as a parameter that describes the rate of molecular mixing between fuel from the respective injections, and its properties are of interest from a modelling perspective.

The objective of this study is to use Direct Numerical Simulation (DNS) to investigate how the entrainment of ambient fluid and the scalar dissipation rates of jet fluid are affected by split injection. To this end, three injection scenarios are simulated and compared: a starting jet, a stopping jet, and a restarting jet.

Split-injection configuration

The simulation configuration involves a round jet of turbulent fluid issuing from a flat plate into a quiescent atmosphere. The injected fluid is an ideal gas with the same density as the ambient fluid. The jet Reynolds number is 7,290 based on the volume flow rate. First, a statistically-stationary solution for the near-field of the turbulent jet is obtained by simulating the jet flow for 620 jet times, where the jet time ($\tau = D/U_0$) is defined by the ratio of the jet inlet diameter (D) and the bulk velocity (U_0). The stopping jet simulation is initialized at $t=0$ with the final solution from the statistically-stationary jet simulation and imposing a jet velocity equal to zero. The restarting jet simulation is initialized from the stopping jet solution 20τ after the stopping transient, as illustrated in Fig. 1. Two mixture fractions, Z_1 and Z_2 are used to distinguish mass of fluid that is injected before and after the jet is restarted. For comparison with the re-starting jet case, a new starting jet simulation is performed, with the impulsively started jet issuing into stagnant flow (not shown in Fig. 1).

Preliminary analysis [12] shows that when the non-dimensional formation time of an injection pulse (defined by the ratio of the pulse duration to the jet time [13]) is greater than twenty, the velocity and mixture fraction profiles in the middle portion of the pulse resemble those

seen at the same downstream location in a statistically-stationary jet with the same Reynolds number. Taking a statistically-stationary jet as the starting point for this study therefore provides an initial condition that is relevant to the majority of Diesel-engine split-injection scenarios that have large formation times.

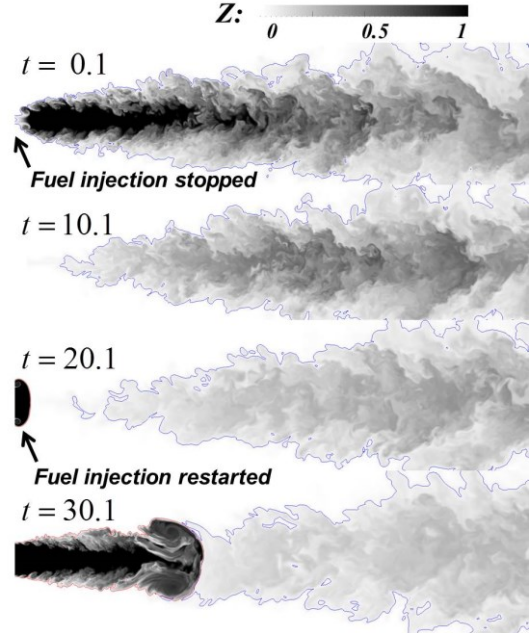


Figure 1. Mixture fraction contours on a cross section through the jet centreline illustrating a stopping jet and a restarting jet. The fuel injection stops at $t = 0$ and restarts at $t = 20\tau$. The blue and red lines represent the isocontours of $Z_1 = 0.05$ and $Z_2 = 0.05$, respectively.

Simulation details

The flow is simulated with the compressible DNS code HiPSTAR, developed by the University of Southampton [14]. A fourth-order finite difference scheme [15] is used in the longitudinal and the radial directions, while the spectral method is used in circumferential direction. A fourth-order low memory Runge-Kutta scheme [15] is used for time advancement. In addition, skew-symmetric splitting of the nonlinear terms is used to enhance the stability [16]. A wave-number-optimized filter is used [17] after each full Runge-Kutta cycle with a 0.2 weighting to remove spurious oscillations.

For the computational mesh, a stretched grid is used, modified from a previous round jet study [14]. The original grid was refined considering the Reynolds number scaling, ($\Delta \sim 1/Re^{3/4}$). In the radial direction, the grid is most refined near the edge of the jet inlet ($r=D/2$) where the velocity and scalar gradients are greatest [14], and 145 points are assigned radially within the jet diameter. In the axial direction, the grid is most refined near the inlet and gradually stretched moving downstream. In the circumferential direction, 64 wave modes are used, corresponding to 130 physical points. The grid consists of 3020x834x130 structured nodes, spanning axially from $x=0-60D$ and radially from $r=0-30D$.

All scalar diffusivities (D_s) are assumed equal with unity Lewis number, and the Prandtl number is set equal to 0.72. If not specified, length, velocity, and time are normalized by the inlet diameter (D), the mean inlet bulk velocity (U_0), and the jet time scale ($\tau=D/U_0$).

The jet issues through a smooth no-slip wall into an open cylindrical domain. A top-hat profile is specified for the jet's mean velocity and for the mixture fraction at inlet. The top-hat profile involves a uniform velocity until $r=0.475D$ and smoothly drops to zero following a half cosine function. Away from the jet inlet ($r>0.5D$), a no-slip wall is imposed at $x=0$. Pseudo-turbulent velocity fluctuations are superimposed at the inlet using the digital filter method [18] and a low turbulent intensity of 3%. All the other boundaries are non-reflecting outlets with a small buffer region at the downstream outlet boundary [19].

In order to accelerate the development of the statistically-stationary jet flow field, the flow is simulated for 540τ using a computational mesh with half of the resolution of the final grid. By 540 jet times the first order and the second order statistics in the first 30 diameters of the domain show that the simulation has reached a statistically-stationary state. Then, the half resolved solution is interpolated onto the final mesh, and the simulation continued over additional 80τ , confirming that statistical-stationarity is established. The converged turbulent jet simulation also displays self-similarity downstream of ten jet diameters as shown in Fig. 2.

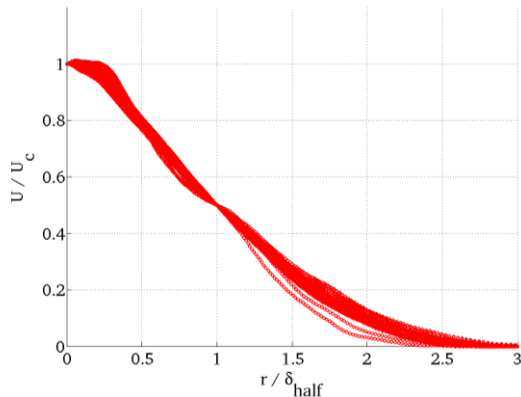


Figure 2. The radial dependence of mean axial velocity scaled by the half radius and the centreline velocity for $x/D = 10-25$.

The simulation results are compared with others reported for the steady state condition. The centerline decay rate shows 6.7, which is consistent with other reported data [20] with a wall inlet and top hat velocity profile. Figure 2 shows the radial dependency of mean axial velocity and

Figure 3 shows the entrainment coefficients defined by Ricou and Spalding [21]. The self-similarity starts to appear from $x>15D$, and the entrainment coefficient matches with the reported data in the self-similar far field of the jet [21].

In order to investigate the ability of Musculus's model [2] to describe entrainment dynamics, Eq. 1 is discretized using a WENO scheme [22] and time integrated using a 3rd order Runge-Kutta scheme [23].

Numerical simulation of Eq. 1 is necessary because the analytical solution presented by Musculus is only applicable when the injection rate decreases linearly.

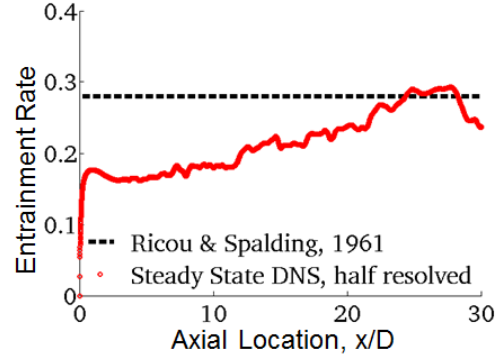


Figure 3. The axial dependence of entrainment coefficient and the far-field value from Ref. [21].

Mass Entrainment

The mass flux at a given axial location is evaluated by integrating the axial velocity in the transverse direction out to three half-radii (the half-radius is the radial location where the mean axial velocity falls to half of the centerline mean velocity). Figure 4 shows the axial dependency of the mass flux at different times for the new starting jet and the restarting jet. The mass flux near the head of the jet has a bell shape. The mass flux at the very front of a starting jet is low because the head of jet pushes fluid away from the centerline. The maximum mass flux region corresponds to the vortex region right behind the head of the starting jet. This vortex core traps a volume of the surrounding fluid and thereby augments the overall mass flux.

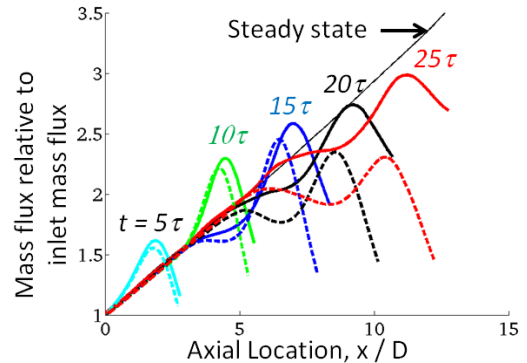


Figure 4. Evolution of the normalized axial mass flux after the (re-)start of injection: dashed lines: new starting jet; solid lines: restarting jet. Injections begin at $t=0$.

Figure 4 also illustrates the difference between the new starting jet and the restarting jet. For example, the maximum mass flux at $t=25\tau$ is 30% greater in the restarted jet compared to the starting jet, and close to the steady-state value. The cause for the difference between the starting and restarting jets can be explained partly by considering Figure 5. Figure 5 shows that subtracting the mass flux in the stopping jet from the mass flux in the restarted jet gives a net mass flux similar to the value in the starting jet. Put another way, the mass flux in the restarting jet is given approximately by summing the

mass flux in the wake of the preceding stopping jet and the mass flux obtained from an impulsive jet issuing into a quiescent flow. The remaining differences may be attributable to the residual turbulence and the induced velocity from the preceding injection pulse. Their combined effect is to reduce entrainment into, and to increase the penetration of the restarting jet.

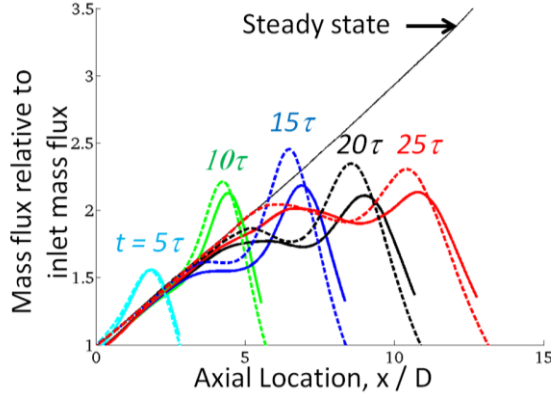


Figure 5. Evolution of the axial mass flux after the (re-)start of injection: dashed lines: new starting jet; solid lines: the mass flux in the stopping jet subtracted from the mass flux in the restarting jet.

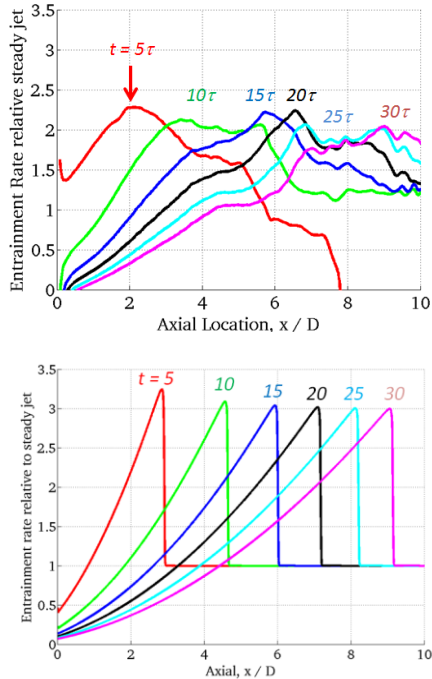


Figure 6. Time evolution of the entrainment rate; (top) DNS results, and (bottom) numerical solution of Musculus's model in Eq. 1 with $\alpha=1$ and $x_0=-2$.

The entrainment rate is given by the axial gradient of the cross-stream integrated mass flux. Figure 6 shows the spatial dependence of the entrainment rate of the stopping jet from the near field of the DNS and from Musculus' model [2]. Quantitative agreement is not expected because Musculus' model applies to the self-similar region further downstream in the jet. However, after

adjusting the jet spreading coefficient α to a value that is representative of the jet development in the near field, a qualitative comparison reveals several points. The overall shape of the entrainment rate is similar. In particular, the model predicts the shallow gradient of the entrainment rate in the tail of the deceleration wave. Differences are as follows: The Musculus model shows a sharp peak in entrainment and a sudden drop at the leading edge of the deceleration wave, while DNS results show a smooth profile with an apparent plateau within the deceleration wave. In addition, Musculus predicted that in the long term behavior, the entrainment rate asymptotes to 3 times the value in a steady turbulent jet, however, DNS results show that the entrainment rate rather asymptotes to 2. These differences may be explained in part by the neglect of axial transport in Musculus' model and his assumption that the jet width remains fixed as the entrainment wave passes.

Fluid entrainment in the stopping vortex

When the fuel injection stops, a stopping vortex is shed at the jet inlet, as shown in Figure 7. This vortex entraps a ring of jet fluid that propagates away from the jet centerline due to the velocity induced by the image vortex. When the jet restarts, the fluid trapped in the stopping vortex is re-entrained. In the case of fuel injection under autoignitive conditions, the fuel contained in the stopping vortex will continue to react and the radicals produced, even in low concentrations, may facilitate earlier ignition when the jet restarts. Further investigation would be needed to establish whether this effect has any significance in a liquid-fueled Diesel engine.

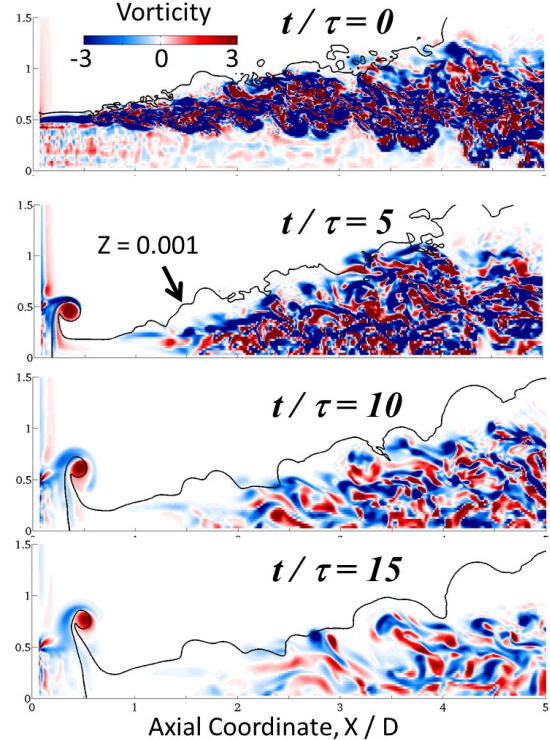


Figure 7. Time evolution of the vorticity and the iso-contour of mixture fraction for the stopping jet.

Evolution of scalar dissipation rate

Figure 8 shows the iso-contours of mixture fractions Z_1 , Z_2 and their cross scalar dissipation rate. The average mixture fractions and cross-scalar dissipation rate were obtained by averaging circumferentially. The area of high cross scalar dissipation rate represents the region where fluid from the two injection events is mixing. The average cross-scalar dissipation rate is mostly negative, indicating that the two mixture fractions' gradients are opposed. A region of increased cross-dissipation is visible close to the jet inlet due to mixing between the old fluid (Z_1) that was trapped in the stopping vortex and the fluid (Z_2) from the second injection.

In the core of the leading vortex, at roughly at $x/D = 6$, there is a region of low cross scalar dissipation rate. In the vortex core, air and Z_2 are present, but the mass fraction Z_1 falls below 1×10^{-4} because the core of the vortex contains ambient fluid that was entrained as the jet started, in the region of low Z_1 close to the inlet. The rotation of the vortex also suppresses mixing with the ambient fluid.

The mixing between the two fuels is the strongest at the head of the jet and in the surroundings of the vortex core as illustrated by the magnitude of the scalar dissipation rate.

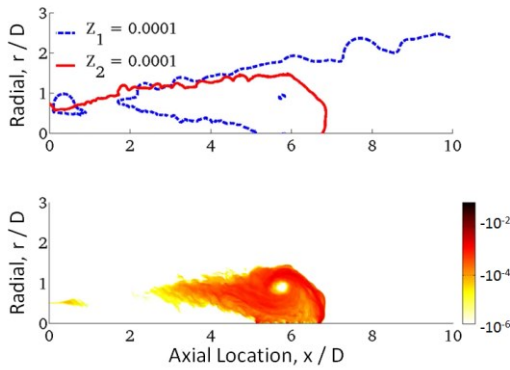


Figure 8. Circumferentially averaged mixture fractions and cross scalar dissipation rate: (top) iso-contours of mixture fractions and (bottom) cross scalar dissipation rate at $t = 26 \tau$.

Figure 9 shows the circumferentially averaged scalar dissipation rate in the new starting jet and the restarting jet at $t=15 \tau$. Again, a region of low scalar dissipation appears at the core of the starting vortex due to the core of entrained ambient fluid, and the suppression of mixing by the rotating flow. The structure of the leading vortex is less clear for the restarting jet – possibly because the turbulent flow left in the wake of the stopping jet acts to enhance mixing and to disrupt the propagation of the starting vortex.

Figure 9 shows the evolution of the circumferentially-averaged scalar dissipation rate along the iso-surface where the mean mixture fraction equals 0.06. This mixture fraction iso-surface corresponds to fluid near the exterior of the jet where ignition and flame

stabilization tend to occur in Diesel engine fuel jets. Figure 10 compares the axial variation of the averaged scalar dissipation rate for the continuous jet, the starting jet and the restarting jet. The head of the fuel jet contains higher scalar dissipation rate than steady state condition. However, the scalar dissipation rate evolves towards the steady-state value as the wave of elevated scalar dissipation rate passes. It is evident in Figure 10 that the head of the wave of elevated dissipation rate travels faster than the trailing edge of the wave, so that the length of the region with elevated dissipation rate extends over time. Further analysis is required in order to understand whether there is a relationship between the propagation of scalar dissipation rate waves and the propagation of entrainment waves.

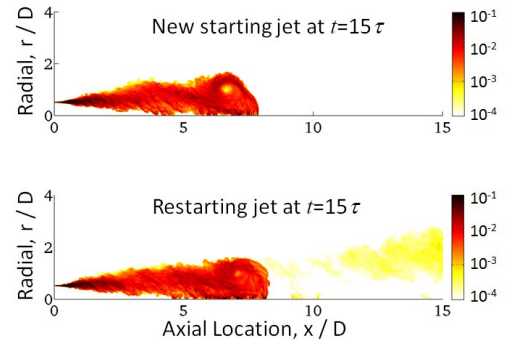


Figure 9. Circumferentially averaged scalar dissipation rate of the new starting jet and the re-starting jet.

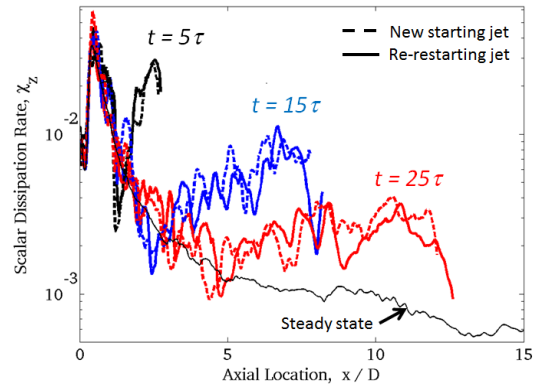


Figure 10. Scalar dissipation rate on the iso-surface of $Z_i=0.06$ in the new starting jet and in the re-starting jet.

The scalar dissipation statistics have been computed from one set of flow realizations and they are subject to statistical noise. Noting that Figure 10 is plotted on a logarithmic scale, it is evident however that the scalar dissipation rate at the head of the new starting jet is significantly greater than in the restarting jet, on average. This difference arises because the restarting jet propagates into the wake of the previous stopping jet so that the restarting jet sees a lower velocity difference compared to the new starting jet, and also because turbulence from the previous stopping jet disrupts structure of the starting vortex and thereby reduces compressive straining of the scalar field.

Because the scalar dissipation rate in the restarting jet is less than in the new starting jet, and because the dissipation rate in the wake of the stopping jet is greater than zero, the dissipation rate in the restarting jet cannot be attributed to superposition of the dissipation rates from the stopping jet wake and the new-starting jet. This observation is in contrast to the additive nature of the entrainment dynamics – highlighting the fundamentally different mechanisms that drive the entrainment and scalar dissipation physics.

Conclusions

The effects of split-injection on entrainment and scalar dissipation are analyzed in a gaseous non-reacting jet with jet Reynolds number of 7290. Using DNS, the effects of starting the jet, stopping the jet and also restarting the jet after a period of 20 jet times have been assessed by comparison with a continuous injection case.

It is observed that the entrainment of ambient fluid is suppressed (enhanced) when the jet velocity increases (decreases) respectively, in agreement with previous studies. In addition, the present results show that the entrainment field observed in the restarting jet may be approximated by superimposing the entrainment field in the new-starting jet onto the entrainment field due to the wake of the stopping jet. The entrainment rate in the stopping jet is in qualitative agreement with one-dimensional entrainment model developed by Musculus, however the profile of the entrainment wave is less sharp and plateaus with a normalized entrainment value of two, as opposed to the value of three predicted by Musculus. It was also noted that a stopping vortex transports a small amount of jet fluid radially outwards from the jet nozzle, and this fluid is re-entrained subsequently when the jet restarts. The impact of this effect in autoignitive fuel jets requires further investigation.

The cross-stream averaged dissipation rate and the dissipation rate in the radially outward fluid (i.e. where ignition occurs in an igniting fuel jet) are enhanced during the starting transient. (The reverse effect is also observed during the stopping transient but not shown in this paper due to space limitations). The increase in the scalar dissipation rate is less in the restarted jet than in the newly-started jet. This difference may arise because the turbulent wake from the stopping jet attenuates the strength of the starting vortex and also reduces the relative velocity between the restarting jet and the surrounding fluid. The vortex core at the head of the starting jet exhibits reduced scalar dissipation, both due to lower concentrations of jet fluid and due to suppression of the turbulent mixing by the rotation.

While entrainment and scalar dissipation are both described as mixing processes and both affect ignition and combustion in pulsed fuel jets, the results of this study highlight the fact that their dynamics are fundamentally different.

Acknowledgements

This work has been performed with support from the EPSRC EP/L002698/1, using resources of the UK National High Performance Computing Facility (ARCHER).

References

- [1] S.M. Kato, B.C. Groenewegen, R.E. Breidenthal, *AIAA J.* 25, (1987) 165–168.
- [2] M.P.B. Musculus, *Journal of Fluid Mechanics* 638 (2009) 117–140.
- [3] J. Craske, M. van Reeuwijk, *Journal of Fluid Mechanics* 763 (2015) 500–537.
- [4] H. Johari, R. Paduano, *Exp. Fluids* 23 (1997) 272–280.
- [5] M.P.B. Musculus, T. Lachaux, L.M. Pickett, C.A. Idicheria, *SAE Trans.* 116(3) (2007) 515–541.
- [6] C.L. Genzale, R.D. Reitz, M.P. Musculus, *SAE International Journal of Engines* 1(1) (2008) 913–937.
- [7] J. Anders, V. Magi, J. Abraham, *Numerical Heat Transfer, Part A: Applications* 54 (2008) 999–1021.
- [8] E. Mastorakos, T.A. Baritaud, T.J. Poinot, *Combustion and Flame* 109 (1997) 198–223.
- [9] N. Soulopoulos, Y. Hardalupas, A.M.K.P. Taylor, *Experiments in Fluids*, 55 (2014).
- [10] N. Peters. *Turbulent Combustion*, Cambridge University Press, 2000.
- [11] C. Hasse, N. Peters, *Proceedings of the Combustion Institute* 30 (2005) 2755–2762.
- [12] D.H. Shin, and E.S. Richardson, *Autumn Meeting of the British Section of the Combustion Institute*, London, United Kingdom, (2014).
- [13] Lakshminarasimhan, K., Clemens, N. T. & Ezekoye, O. A. *Exp. Fluids* 41 (2006) 523–542.
- [14] R. Sandberg, N. Sandham, V. Suponitsky, *International Journal of Heat and Fluid Flow*, 35 (2012) 33–44.
- [15] C.A. Kennedy, M.H. Carpenter, R.M. Lewis, *Applied Numerical Mathematics* 35 (2000) 177–219.
- [16] C.A. Kennedy, A. Gruber, *Journal of Computational Physics* 227 (2008) 1676–1700.
- [17] C. Bogey, N. de Cacqueray, C. Bailly, *Journal of Computational Physics* 228 (2009) 1447–1465.
- [18] E. Toubert, N. Sandham, *Theoretical and Computational Fluid Dynamics* 23 (2009) 79–107.
- [19] T.J. Poinot, S.K. Lele, *Journal of Computational Physics* 101 (1992) 104–129.
- [20] T. H. Weisgraber, D. Liepmann, *Experiments in Fluids* 24 (1998) 210 – 224.
- [21] F.P. Ricou, D.B. Spalding, *Journal of Fluid Mechanics* 11 (1961) 21–32.
- [22] G.S. Jiang, D.P. Peng, *Siam Journal on Scientific Computing* 21 (6) (2000) 2126–2143.
- [23] S. Gottlieb, C.W. Shu, *Mathematics of Computation* 67 (221) (1998) 73–85.